An original combined method for electrical conductivity measurement of polymer composites under extensional deformation

Marjorie Marcourt, Philippe Cassagnau, René Fulchiron, Dimitri Rousseaux, Olivier Lhost, Simon Karam

An Innovative Combined Method for Electrical Conductivity Measurement of Polymer Composites under Extensional Deformation.

Marjorie Marcourt, Philippe Cassagnau, René Fulchiron[a)],

Univ Lyon, Université Claude Bernard Lyon 1, CNRS UMR 5223, Ingénierie des Matériaux Polymères, F-69622, Villeurbanne Cedex, France

Dimitri Rousseaux, Olivier Lhost, Simon Karam

Total Research and Technology Feluy Zone Industrielle Feluy C 7181 Feluy, Belgium

[a)]Corresponding author : rene.fulchiron@univ-lyon1.fr

Abstract:

In the last decades, nanocomposites made of polymer matrix filled with CNT have been a great topic of studies, particularly as concerns the rheological behavior and the electrical characteristics under shear. In contrast, this work focuses on the deformation of the CNT network in elongated polymer melts by a combination of conductivity monitoring and extensional rheological measurement. For this specific purpose, an Extensional Viscosity Fixture accessory of a rotational rheometer ARES has been modified to allow the sample conductivity measurement. This new set-up gives access to the measurement of the electrical conductivity simultaneously with the extensional stress under extensional deformation. First results have shown that the conductivity of CNT/polystyrene nanocomposites can present a sharp decrease before the sample break and this decrease appears more rapidly for higher extensional rates and lower temperatures. The results have been correlated to experimental conditions via the introduction of the Weissenberg number.

1. Introduction

The addition of Carbon Nanotubes (CNT) to a polymer matrix has paved the way of ultra-low filled nanocomposites characterized by both electrical and mechanical specific properties generally due to the percolation network formed by the fillers [1-3]. From the abundant literature on the topic, some general trends can be recalled. Theoretically, the large aspect ratio (*L/d*) leads to nanocomposites with an insulator/conductor transition for an ultra-low filler amount. However, this achievement of nanocomposites with tailored conductivity properties remains a challenge. As CNT are fillers with dimension in the range of polymer chains size, the interactions are predominant. Therefore, the mixing and the dispersion processes of CNT in the polymer matrix are crucial issues in elaborating the nanocomposites and thus, in controlling its properties [4-7]. Moreover, after its elaboration, the material may be subjected to a very large deformation during the forming process (thermoforming, injection molding, melt blowing…) leading to a possible modification or destruction of the network. In this regard, the present study is devoted to the analysis of the electrical behavior of nanocomposites submitted to extensional forces.

Electrical properties are governed by the filler dispersion state and the filler-filler connection. Indeed, when fillers are too well dispersed, the material will present a poor electrical conductivity as

these fillers do not constitute an electron pathway. A good, electron conductor network is made of homogeneously dispersed and CNT aggregates interconnected together [8-11]. However, well above T_g the flow can drastically modify the filler structure through aggregation and disaggregation mechanisms and, consequently affect the electrical properties of the final parts [8, 12, 13]. In order to understand those phenomena, a great number of studies have been carried out on nanocomposite with highly viscous polymer matrix like Skipa *et al*.[14] and Pegel *et al*. [11] (PMMA/ CNT), Abbasi *et al.*[15] (PC/MWCNT) and Kota *et al*. [16] (PS/MWCNT). Other studies are reported on low viscous thermoplastic or uncured thermoset resin filled with CNT [8, 17, 18]. Using a rheometer set-up with DC conductivity monitoring, they have highlighted distinct conductivity variations revealing the filler network evolution. For well dispersed and distributed fillers (electrically insulating material), a quiescent annealing at temperature above T_g will lead to a significant conductivity increase. Through diffusion and filler-filler interactions, the formation of the percolated network will be triggered. Under external forces the mechanism is more complex illustrating the different variation obtained. The majority of reported studies carried out on highly viscous systems have highlighted a conductivity decrease under both high and low shear stresses. Under shear stresses, the fillers connections break and the aggregates are subjected to some erosion. However, Hilarius *et al*. [6] have dealt a consistent work in this field. They have shown that, under a low steady shear of $0.02s^{-1}$, the conductivity of the material can decrease until it reaches an equilibrium state and can even increase. Those phenomena have been attributed to the superposition of buildup and destruction of connections.

However, during industrial processing, the nanocomposite materials undergo huge shear and elongation strains at very high rate. This explains why the industrialization of nanocomposites with tailored conductivity remains a thorny challenge.

A few studies have been carried out on nanocomposites under high deformations. Abbasi *et al*. [19] have observed a slight orientation of the filler after micro injection of nanocomposite. In other works, fibers of CNT/Polyamide 12 have been obtained by melt spinning to induce high deformation and show its impact on electrical properties. A huge conductivity decrease was obtained depending on the strain rate and the strain applied [20]. Under high shear and extensional rates, the filler network experienced stronger deformation which is transmitted to the aggregate scale: the aggregates are separated but also stretched.

In contrast to all studies carried out on the electrical conductivity monitoring of nanocomposites materials submitted to shear, the present work focuses on extensional deformation. To go further in the comprehension of network deformation/destruction under extensional flow, a commercialized Extensional Viscosity Fixture (EVF) system has been modified to monitor the electrical properties of nanocomposites, together with the extensional viscosity during the melt deformation. As the polymer matrix is electrically insulating, the measured current is characteristic of the CNT network giving the opportunity to follow the network evolution under extensional forces.

2. Experimental section

2.1 Materials

The fillers used are Multi Wall Carbon Nanotubes Nanocyl^{TM} NC7000 supplied by Nanocyl S.A Belgium. They have a diameter (*d)* of 9 nm and a length distribution (*L)* mainly between 100 nm and 2 µm. The matrix is a pure Polystyrene Crystal 1160 (PS) supplied by Total Petrochemicals. The

nanocomposites were prepared from a masterbatch of PS filled with 15wt% MWCNTs and diluted with the pure PS to reach the desired concentration [21].

2.2 Characterization

a) Scanning Electron Microscopy

The filler dispersion has been investigated by Scanning Electron Microscopy (SEM) using a device LSM800 from Zeiss. The detection was ensured owing to in-Lens detector which is located inside the beam focusing lens. The observations have been carried out with a distance between the surface sample and the final condenser lens (the working distance WD) of around 5 mm, an aperture size fixed at 30µm and the accelerating voltage ranging from 15kV to 20kV. As the in-Lens detector is very sensitive to surface roughness, the sample surface has been cut with diamond knife to remove any roughness and promote the contrast between electrically conductor filler and insulating matrix. This observation technique will be not detailed in the paper; however the reader can refer to studies on this method [22-24].

b) Electrical Characterization

Electrical properties analysis has been conducted on compression molded samples with a post annealing at 200°C for 20 min. This ensures a thermodynamically equilibrium state with a well – developed filler network. Colloidal silver paste is applied on the surface sample to obtain a good electrical contact between the electrodes and the materials. Owing to a Keithley 237 power supply a 10 volt DC is delivered and the current passing through the sample is measured.

c) Dynamic rheology

Rheological experiments in dynamic frequency sweep mode with parallel plates geometry (25mm) were performed using an ARES rheometer (TA instruments) at various temperatures between 200°C and 240°C under nitrogen atmosphere. The master curves were constructed at a reference temperature of 200°C (see Figure 1). In addition, the master curve obtained for the sole PS was fitted with a classical Maxwell N modes model [25] as:

$$G'(\omega) = \sum_{i=1}^{N} \frac{G_i \omega^2 \lambda_i^2}{1 + \omega^2 \lambda_i^2}$$	**Equation 1**
$$G''(\omega) = \sum_{i=1}^{N} \frac{G_i \omega \lambda}{1 + \omega^2 \lambda_i^2}$$	**Equation 2**

where G_i is the modulus contribution corresponding to the relaxation time λ_i. The λ_i parameters were fixed over the range of time constants corresponding to the reverse of the experimental frequency range and the G_i were obtained by means of an iterative method minimizing the following criterion [26]:

$$\sum_{j=1}^{M} \left(\frac{G'(\omega_j)}{G_j' - 1} - 1\right)^2 + \left(\frac{G''(\omega_j)}{G_j'' - 1} - 1\right)^2$$	**Equation 3**

where M is the number of G_j' and G_j'' experimental values. The number of modes was fixed to 5 as the best compromise between satisfying fit of the experimental curves and physically proper values of the G_i (no negative modulus contribution).

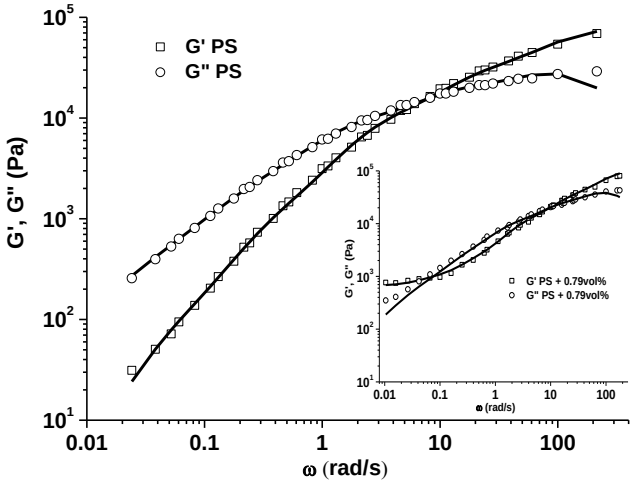

Figure 1 : Master curve for PS at a reference temperature of 200°C. The inset represents the master curve fo PS filled with 0.79 vol% of CNT at the same reference temperature. Experimental data G'(□) and G"(○) fitted by a discrete Maxwell model (solid line).

Moreover, concerning the relaxation spectrum, since the λ_i values were arbitrarily chosen, it would be meaningless to consider a relaxation mechanism associated to each of these values. That is why it is more appropriate to handle meaningful values as the number or weight average relaxation times, (respectively, λ_n and λ_w) [27] that are deduced from the λ_i and G_i parameters by Equation 4 and Equation 5.

$\lambda_n = \frac{\sum_{i=1}^{n} G_i \lambda_i}{\sum_{i=1}^{n} G_i} = \frac{\eta_0}{G_N^0}$	**Equation 4**
$\lambda_w = \frac{\sum_{i=1}^{n} G_i \lambda_i^2}{\sum_{i=1}^{n} G_i \lambda_i} = \eta_0 J_e^0$	**Equation 5**

From the building of the master curves, the shift factors a_T were determined and it was verified that they fulfill the WLF (Williams-Landel-Ferry) equation [26, 27]:

$\log(a_T) = \frac{-C_1^0 (T - T_{ref})}{C_2^0 + (T - T_{ref})}$	**Equation 6**

For pure PS, the WLF coefficients C_1^0 and C_2^0 are respectively 3.5 and 1.1x10^2 K for a reference temperature T_{ref} fixed to 200°C.

The zero shear-viscosity η_0 at 200°C is 1x10^4 Pa.s, the compliance J_e^0 is 4x10^{-4} Pa^{-1} and the modulus G_N^0 is 7x10^4 Pa. In the literature it can be found a modulus G_N^0 equal to 2x10^5 Pa [28]. The lower value experimentally obtained can be explained by a larger molecular weight distribution.

The relaxation times at other temperatures can be deduced from the relaxation time of the reference temperature and the shift factor by Equation 7 [25]. The values obtained for the temperatures used for extensional experiments are displayed in Table 1.

$$\lambda_{n-w}(T_0) = \frac{\lambda_{n-w}(T_1)}{a_{T_1}} \quad \text{Equation 7}$$

Table 1 : Rheolgical parameters of pure Polystyrene obtained with a T_{ref} fixed to 200°C

T°C	λ_n (s)	λ_w (s)	a_T
200	1.42×10^{-1}	4.19	1
180	8.74×10^{-1}	26.2	6.24
170	3.11	93.2	22.2
160	16.2	4.83×10^{2}	1.15×10^{2}

The calculated relaxation times are truly wide-ranging. However, the weight average relaxation time is generally considered as more reflecting of the polymer behavior than the number average relaxation time. As a matter of fact, it contains the effect of both the average molar mass and the molar mass distribution [29, 30]. Moreover, it is more linked to the behavior in the terminal zone and, in that sense, is closer to the longest relaxation time of the polymer. Thus, in the following, only the weight average relaxation time will be considered.

2.3 Extensional Viscosity Fixture with conductivity set-up

Extensional experiments were carried out with a commercialized EVF (TA instruments) mounted on the ARES rheometer. This set-up is based on the Meissner concept [31]. It is composed of two drums: a fixed one connected to the torque sensor allowing the measure of the elongational force, and a rotating one moving on a circular orbit centered on the fixed drum. The edges of the sample are fixed on each drum. Using such a system, the extensional rate $\dot{\varepsilon}$ is defined as:

$$\dot{\varepsilon} = \frac{\dot{\theta}(t)R}{L_0} \quad \text{Equation 8}$$

$\dot{\theta}$ is the angular rotation speed, *R* is the drum radius and L_0 is the distance between the two drums. The drums are first heated at the working temperature, and then a sample having dimension of 25x10x0.5 mm^3 is placed and clamped onto the drums. The sample is maintained for around 100 s from the moment when the chamber has reached the working temperature again. This allows the sample relaxation and the sagging effect prevention. Before starting the experiment the sample is pre-stretched at $\dot{\varepsilon} = 0.001\ s^{-1}$ for 10 s .The limit of the system is reached after ¾ of a revolution; just before that the sample comes into contact with itself. As a result, the highest Hencky ε strain reachable is limited to about 4. For their characterization, the samples are taken off right after the end of the test. They are rapidly cooled down with compressed air to avoid any relaxation of their structures.

Home-made modifications have been carried out on the commercialized EVF system to give access to the conductivity measurement. First, the two metallic drums have been electrically isolated

to avoid any short-circuit. Copper thin film with 10 mm width has been rolled around each drum to form electrodes. The two drums are electrically powered with electric cables connected to a Keithley 237 power supply delivering a DC 10V and measuring the resulting current.

The sample is clamped between the two drums and closes the electrical circuit so that the measured current is the current passing through the sample. With temperature higher than T_g the sample fits closely the drums giving a good and homogeneous electrical contact between the sample surface and the electrodes. Figure 2 illustrates the experimental set-up with *A(t)* representing the sample thickness as a function of *t*.

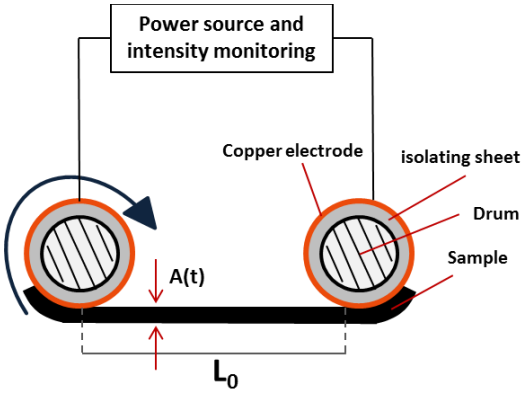

Figure 2 : Cross section view of the experimental set-up.

The potential difference is taken at the distance noted L_0 between the two drums which remains unchanged as the sample is rolled up on the electrode. The time-dependent conductivity is deduced from the measured current as:

$$\sigma(t) = \frac{1}{\rho} = \frac{L_0 . I(t)}{U . S(t)} \qquad \textbf{Equation 9}$$

, where L_0 is the sample length between the drums, *I(t)*is the measured current, *U* the applied DC voltage, and *S(t)* the effective cross-section area of the sample. Assuming a uniform deformation of the sample and a constant volume this area can be expressed as a function of time and the initial section S_0 as:

$$S(t) = S_0 e^{-\varepsilon_H} = S_0 e^{-\dot{\varepsilon} t} \qquad \textbf{Equation 10}$$

Combining Equation 9 and Equation 10, the conductivity, as a function of time, can be expressed by:

$$\sigma(t) = \frac{L_0 . I(t)}{U . S_0 e^{-\dot{\varepsilon} t}} \qquad \textbf{Equation 11}$$

Samples were deformed at strain rates between $0.005 \leq \dot{\varepsilon} \leq 0.1\ s^{-1}$. These values are taken small enough to facilitate the electrical acquisition and to monitor the structure evolution of the conductor network. The conductivity monitoring configuration makes possible reliable measurements for high Hencky deformations. Indeed, for Hencky deformation around 2 the electrical cables prevent the

drum to rotate and, by consequence, a false upturn of the stress is obtained whereas it is not measured without the wire (see Figure 3).

First, the conductivity monitoring has been tested on systems with a relatively high initial electrical conductivity. A satisfying reproducibility test is presented in Figure 3. The conductivity variation and the extensional viscosity displayed in Figure 3 were carried out at 160°C with an extensional rate of 0.01s^{-1} on the same system: PS filled with 0.79 vol% CNT. For the sample 1 (S1) and the sample 2 (S2) the measurements were carried out with the electrical system whereas, for the sample 3 (S3), it was conducted only with the classical EVF device. The extensional stresses of S1 and S2 highlight the deviation from the EVF systems due to the electrical cables which prevent the drum rotation (see Ext. Stress S1 and S2 in Figure 3).
For the following, in order to discriminate the samples behavior, two characteristic strain values are defined: ε_b and ε_σ. They represent respectively the Hencky deformation at the sample break and the Hencky deformation when the conductivity falls down and reaches 10^{-6} S/cm (taken arbitrarily).

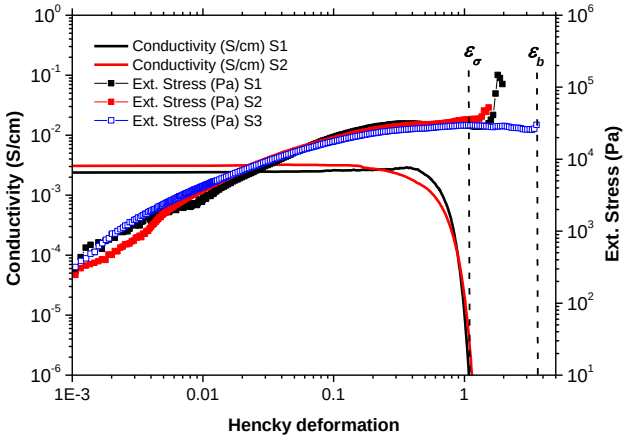

Figure 3 : Polystyrene filled with 0.79 vol% of CNT deformed at 160°C under extensional rate fixed to 0.01s^{-1} The extensional stress curves S3 has been monitored on a EVF without the electrical set-up to reach higher Hencky deformation and highlights the impact on the electrical set-up on the stress monitoring (see S1 and S2).

In Figure 3 the conductivity strain limit ε_σ presents a deviation of +/- 0.1. At higher extensional rate, for instance $\dot{\varepsilon}$ = 0.1 s^{-1}, ε_σ presents a slightly higher deviation of +/- 0.24. Those deviations remain relatively low and illustrate the good reproducibility of this set-up.

In addition to the reproducibility, it is necessary to check that the experimental set-up does not take part in the filler deformation and orientation by electrophoresis mechanism as experienced by Martin *et al.*[17]. To do so, the hydrodynamic forces must be compared to the electrostatic polarization force. The hydrodynamic force acting on a spherical particle (here an aggregate) can be expressed as:

$F_H = 6\pi\eta_0 a^2 \dot{\varepsilon}$	**Equation 12**

with η_0 the zero shear viscosity of the pure matrix, a the radius of the particle and $\dot{\varepsilon}$ the strain rate. On the other hand, the electrostatic polarization force exercised on a spherical particle is expressed as:

$F_E = 12\pi\varepsilon_0\varepsilon_r a^2\beta^2 E^2$	**Equation 13**

where ε_0 = 8.8542 x 10^{-12} F/m is the permittivity of the free space, ε_r is the relative dielectric constant of the continuous phase, a the particle radius, β is the relative polarizability [= $(\sigma_f-\sigma_p)/(\sigma_f-2\sigma_p)$]where σ_p and σ_f are the conductivity of respectively the polymer phase and the filler. E is the electric field fixed to 1kV/m. Combining Equation 12 and Equation 13 the Mason number (M_n) [32]may be defined as:

$M_n \equiv \frac{F_H}{F_E} = \frac{\eta\dot{\varepsilon}}{2\varepsilon_0\varepsilon_r\beta^2 E^2}$	**Equation 14**

In the present experimental system, for extensional rates in the range of 0.005 s^{-1} to 0.1 s^{-1} the M_n factor is much greater than 1. Therefore, it can be concluded that the electric field does not take part in the fillers alignment and will be neglected in the study.

3. Results

3.1 CNT dispersion and resulting electrical properties

Carbon nanotubes are rod-like shape fillers. Without any functionalization, the surface energy is predominant and forces them to form aggregated structures. SEM observations have been performed on the nanocomposite made of PS filled with 0.79 vol% of CNT. The obtained picture reveals bright and dark areas. The bright areas highlight the electrically conductor fillers: privileged area for secondary electron emission. The dark area is the insulating matrix. This observation method will not be detailed in the paper; however the reader can refer to studies on this method [22-24]. It is relevant to note that the brightness between all aggregates is not homogeneous. This is explained by the depth penetration of the incident electrons. The electron flow will be more important for aggregates near the surface sample (bright area) than the aggregates located deeper in the material (grey scaled area).

Those observations give access to the 2-D picture of the filler dispersion. In Figure 4, a percolated network of CNT in the PS matrix can be observed. The structure obtained is homogenous and does not present any preferred orientation. For the 0.79 vol% CNT material, there is no isolated CNT, so it can be assumed that the system has reached its fully aggregated structure. All the entities seem to take part to the electrons conductive path.

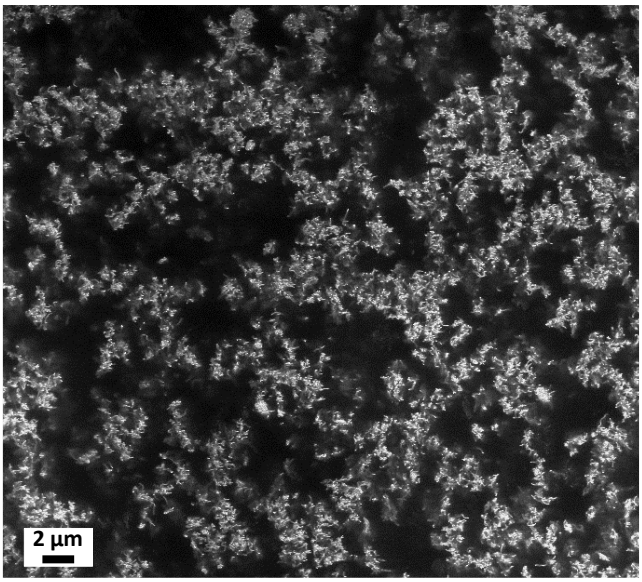

Figure 4 : SEM observation with in-Lens detector, WD fixed at 5.4mm, ETH = 20kV, magnification x2000 of PS filled with 0.79 vol% CNT (compression molded).

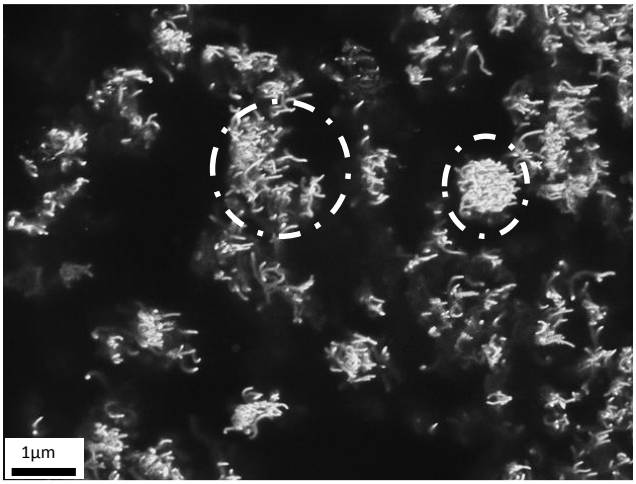

Figure 5 : SEM observation at higher magnification x10 000 of PS filled with 0.79 vol% of CNT (compression molded).

Details of the structure can be observed at higher magnification (see Figure 5). This structure can be outlined as a population of aggregates and agglomerates interconnected together by smaller structures (i.e. small disentangled bundles). In Figure 5, the dense aggregates are highlighted by white dotted circles.

Considering CNT as rods, the number of element per unit volume can be estimated. The volume occupied by a rod can be assimilated to a cylinder. The number of element per unit volume deduced as $\nu = \frac{\Phi}{V_{cylinder}}$ can be used to determine the regime of the system. For the analyzed concentration (max 0.9 vol%), ν is between the ratio $1/L^3$ and the ratio $1/dL^2$ [33]. Thus, the system can be considered in semi-dilute regime. The isolated particles cannot diffuse or rotate freely as the interactions from their closest neighbors are not negligible. This assumption would be only valid for isolated CNT or much disentangled small aggregates or bundles. As for the bigger aggregates and agglomerates, they cannot rotate or diffuse easily. They experience too large hydrodynamic friction forces.

To sum up, the system is made of aggregates and agglomerates with low mobility and more mobile small entities responsible of the connection between aggregates and agglomerates. The state of these small entities will govern the conductivity of the system.

With the addition of fillers, the connections between clusters become predominant, and by consequence, the formed percolated network is more electrically conductor. The conductivity evolution with the filler concentration illustrates this phenomenon (see Figure 6)

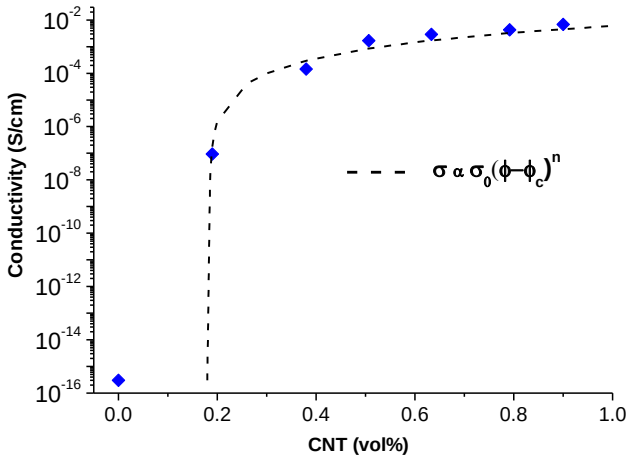

Figure 6 : Evolution of the volume conductivity of PS filled with CNT in function of the filler concentration (measured on compressed samples).The dash dotted line illustrates the percolation threshold law.

The electrical characterization of the different nanocomposites highlights the electrical insulator-conductor transition at very low filler concentration. Using a classical percolation law as $\sigma \propto \sigma_0(\varphi - \varphi_c)^n$, with φ_c the filler concentration at the percolation threshold, the formation of the conductive path can be determined. Here, the electrically insulator-conductor transition occurs for a concentration around 0.18 vol%. The concentration of 0.79 vol% that is largely above the percolation threshold will be especially used for the experimental tests carried out with the new set-up.

3.2 Nanocomposites under extension deformation

The different materials introduced before have been characterized with a common EVF device. For the range of CNT concentration, the extensional rheological measurements present no dependency on the filler concentration. This motivates the coupling of the EVF accessory with conductivity measurement in order to highlight the network variation under extensional deformation.

a) Conductivity variation under extensional deformation

In Figure 3 the variation of the conductivity is plotted as a function of the Hencky deformation. This test has been carried out on samples filled with 0.79 vol% of CNT at 160°C and an extensional rate fixed at 0.01 s^{-1}. First, it is relevant to note that ε_σ is far lower than ε_b. A smooth decrease of the conductivity is triggered at a strain of around 0.15. Then, the conductivity keeps on decreasing until the system reaches a conductor-insulator transition. This experiment highlights the highest uniaxial extensional deformation that the system can endure before becoming electrically insulator. This is a first distinction from the studies carried out under steady shear [14]. Indeed, under shearing, the conductivity can reach a stable non-zero value resulting from the establishment

of an equilibrium regime between destruction and restructuration mechanisms or it can just plummet. Under extensional stresses, the aggregates are dragged apart from each other and stretched in the deformation direction causing the break of the inter-aggregates connections. The structure obtained after a uniaxial deformation of ε=1 is presented in Figure 7.The white arrow indicates the deformation direction. The aggregates network is oriented and deformed within the flow direction (see white circle). However, some aggregates present no preferential orientation or deformation (see white dotted circle in Figure 8). This confirms the assumption introduced in the first section. Indeed, only isolated carbon nanotubes or highly disentangled bundles presenting a structure more flexible can be deformed under external forces.

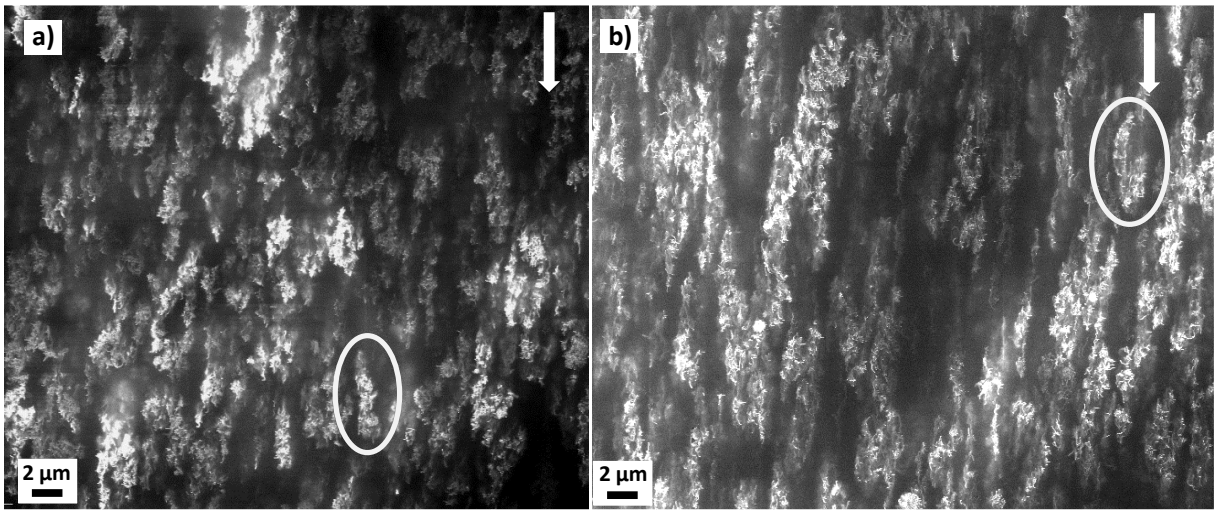

Figure 7 : SEM observation with in-Lens detector 20kV, WD=5mm, magnification x2 000. PS filled with 0.79 vol%of CNT after 1 Hencky deformation at 160°C at an extensional rate of 0.01s^{-1} a) and 0.1 s^{-1} b) respectively.

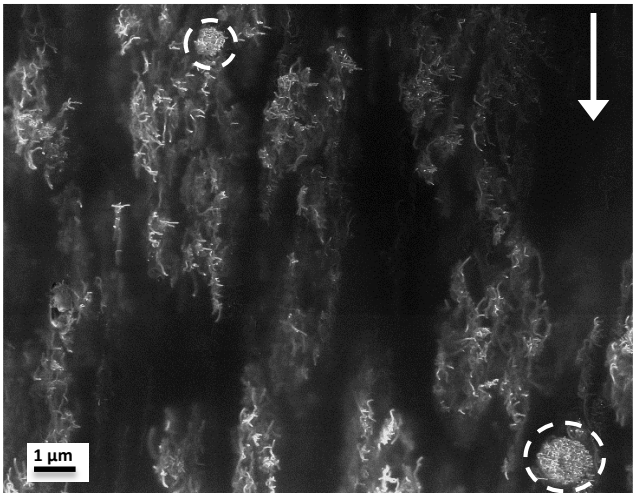

Figure 8 : SEM observation with in-Lens detector 20kV, WD=5mm, magnification x5 000. PS filled with 0.79 vol%of CNT after 1 Hencky deformation at 160°C at an extensional rate of 0.1 s^{-1}.

The deformations implied under extensional stresses are more effective than those occurring under shear. However, stopping the deformation before reaching the critical ε_σ gives rise to the recovery of the sample' conductivity. This result has been obtained from a two-step experiment which is illustrated in Figure 9. The samples are first deformed at an extensional rate fixed to 0.01s^{-1}

at, respectively 160°C, 170°C and 180°C. Then, the deformation is stopped at 1Hencky for the experiment carried out at 160°C, 1.4 for the one carried out at 170°C and 1.8 for the last one carried out at 180°C. These deformations were chosen to obtain approximatively the same conductivity decrease. Finally, the samples are subjected to a quiescent annealing at the same temperature (160°C, 170°c and 180°C respectively). The conductivity recording is continued during this quiescent treatment. To characterize the structural evolution during this quiescent treatment, SEM observations have been carried out before and after the quiescent treatment (see Figure 9).

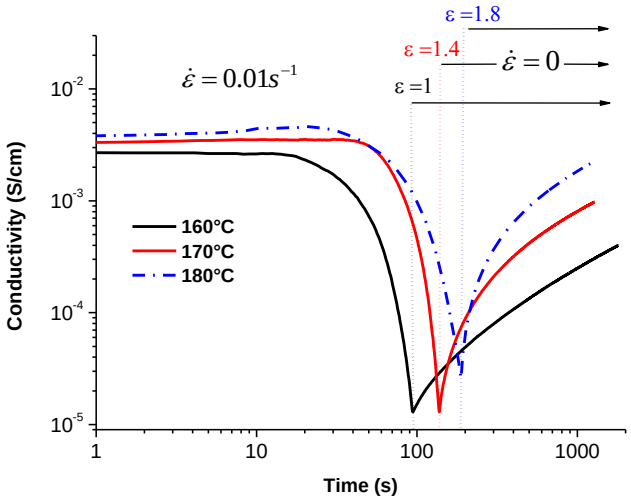

Figure 9 : A two-step extensional experiment carried out at 180°C (PS filled with CNT 0.79vol%). First, an extensional deformation at a rate of 0.01s^{-1} to 1 Hencky and 1.8 Hencky respectively, followed by a quiescent treatment at the same temperature.

As it can be seen in Figure 9, the conductivity starts to increase right after the deformation interruption. The conductivity value when the quiescent treatment starts is respectively 2.5 x10^{-5} S/cm at 180°C and1.3 x10^{-5} S/cm at both 170°C and 160°C.Those close starting values enable the comparison between the three experiments. The conductivity recovery is significantly faster at higher temperature. Because of the very long duration of the total recovery, the conductivity measurement has been stopped before being stabilized. Anyway, this type of experiment illustrates the reversibility of the CNT network damaging mechanism. Other tests have been carried out by stopping the deformation at different Hencky values where the conductivity ranged between 10^{-3} and 10^{-6} S/cm. All have shown the same recovery mechanism which is illustrated in Figure 10.

The structures obtained respectively at 160°C and 1 Hencky and at 180°C and 1.8 Hencky are utterly similar. The agglomerates are stretched and oriented within the flow direction. However, after the quiescent treatment the structures obtained are significantly different and illustrate the conductivity variation in Figure 9. At 160°C; the structure after the quiescent treatment is still oriented within the flow. Under higher temperature, the aggregates are significantly less stretched and the network orientation is less pronounced.

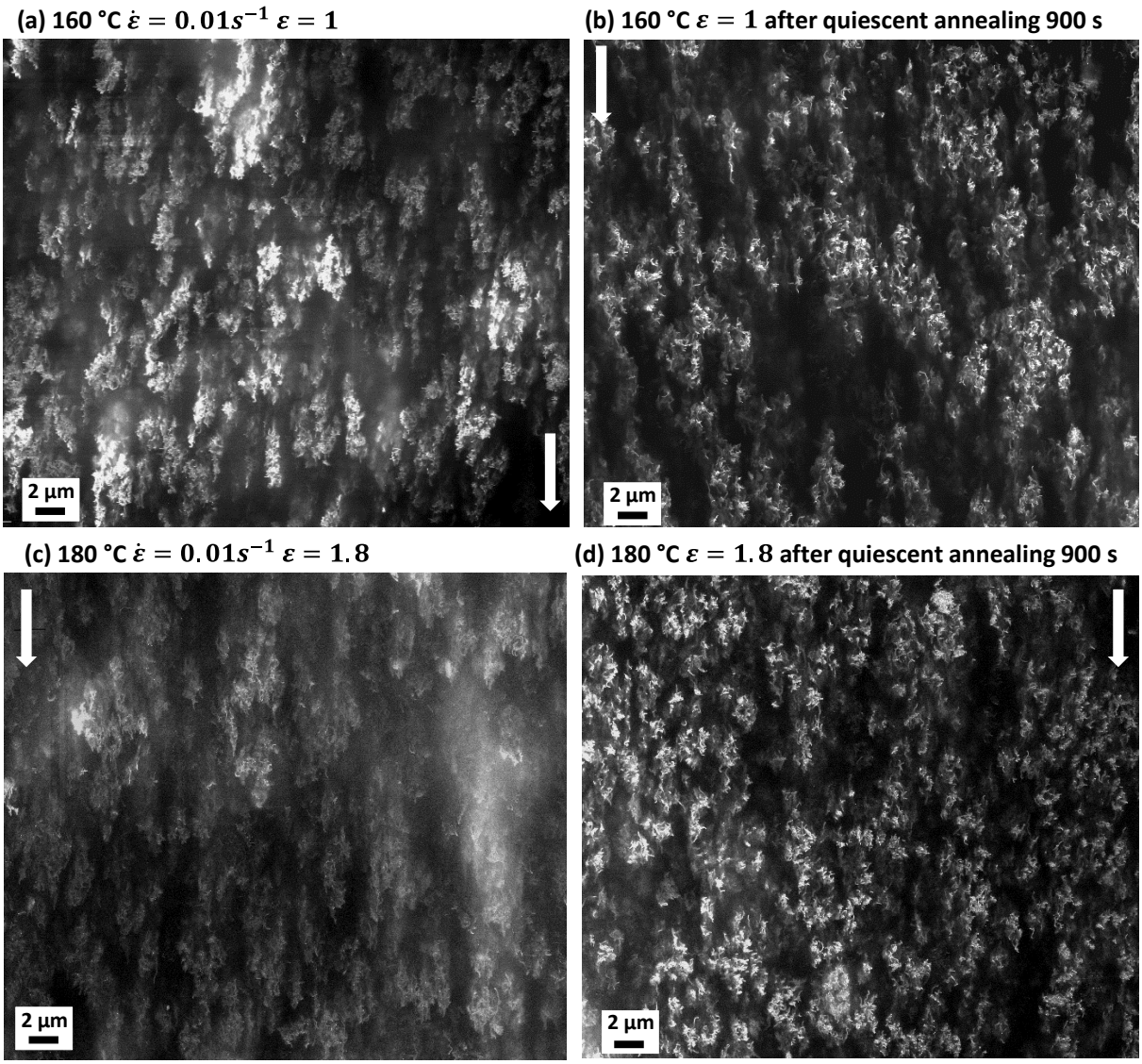

Figure 10 : SEM observation with in-Lens detector 20kV, WD=5mm, magnification x2 000. (a) and (b) structural evolution of PS filled with 0.79 vol% of CNT after 1 Hencky deformation at 160°C at an extensional rate of 0.01 s^{-1}: (a) immediately after elongation, (b) after quiescent annealing at 160°C during 900s., (c) and (d) structural evolution after 1.8 Hencky at 180°C at an extensional rate of 0.01 s^{-1} : (c) immediately after deformation, (d) after quiescent treatment at 180°C during 900s.

The conductivity recovery has also been observed in others studies carried out on nanocomposites under quiescent conditions [11, 14]. This phenomenon is explained by the restoration of connections between aggregates. However, the driven forces are not well understood. In order to understand the network structure evolution during the quiescent step the master curve of the quiescent annealing has been built. The three curves have been set to the same starting point to facilitate the building of the master curve at a T_{ref} fixed to 170°C (see Figure 11). The $a_{T\sigma}$ (shift factor for the quiescent experience) are deduced from the building of the master curve and they fulfill the WLF. The obtained WLF coefficients $C_1^0$and $C_2^0$are respectively equal to 4.8 and 87 K for a T_{ref} fixed to 170°C. For practical reasons, the experiments couldn't have been carried out at 200°C. However, from the obtained WLF coefficients the coefficients at a different reference temperature can be deduced [26, 27]. For a temperature of 200°C, C_1' and C_2' are respectively equal to 3.6 and 1,2x10^2 K. They can henceforth be compared to the WLF coefficients C_1^0 and C_2^0 obtained from the master curve built at a T_{ref} fixed to 200°C (see part c) **Dynamic rheology**) equal to respectively, 3.5 and

$1.1x10^2$ K. The WLF coefficients obtained from the master curve of the quiescent experiment are significantly closed to those obtained in dynamic rheology at the same T_{ref}. This result is meaningful and highlights the prevailing role of the polymer viscoelasticity for the network restructuration. After the deformation, the polymer phase tends to reach an equilibrium state via chains relaxation mechanism. This gives mobility to the filler network and triggers the restructuration. The molecular dynamic will be tackle more specifically in dynamic regime in the last section.

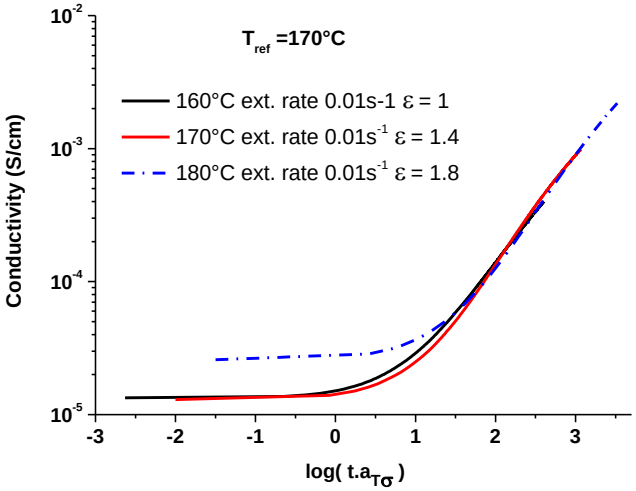

Figure 11 : Master curve of the conductivity recovery during quiescent step build at a T_{ref} fixed to 170°C

In addition, materials with varying amount of CNT have been tested. In Figure 12 is plotted the evolution of ε_σ and ε_b for different CNT concentrations obtained at 160°C with an extensional rate fixed to $0.01s^{-1}$. First of all, it is relevant to point out that for all the tested concentrations, the conductivity limit ε_σ is reached before the sample breaks. The difference between ε_σ and ε_b is quite significant and shows that the frailty of the CNT network is the real limiting factor for manufacturing conductive parts by thermoforming. With the addition of CNT, a slight but significant increase of ε_σ is observed (x2) whereas ε_b is practically unchanged. This highlights the capacity of more filled materials to undergo uniaxial elongation.

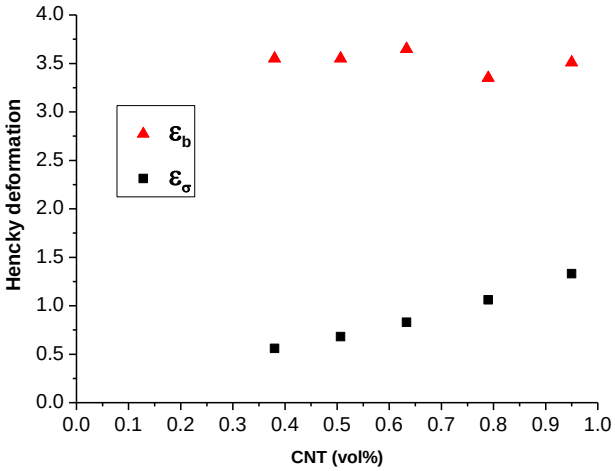

Figure 12 : Evolution of ε_σ and ε_b as a function of CNT concentration. Experiments carried out at 160°c with an extensional rate of $0.01s^{-1}$

b) Influence of the temperature during extensional deformation

The influence of the temperature has been briefly highlighted in the previous section in Figure 9. In this section, its influence will be more specifically investigated on the PS filled with 0.79 vol% material. For this purpose, the material has been tested at three distinct extensional rates for two specific working temperatures: 160°C and 180°C. Figure 13 shows experiments carried out at, respectively 160°C (a) and 180°C (b).

First of all, the extensional rate plays a non-negligible role in the ε_σ values. Indeed, for both temperatures tested, the decreasing of the extensional rate leads to a shift of ε_σ to higher Hencky deformations. This is even more significant at 180°C as illustrated in Figure 13 (b). Indeed, at this temperature, the conductivity variations for extensional rates of $0.005s^{-1}$ and $0.01\ s^{-1}$ are truly contrasting with the variation obtained with an extensional rate of $0.1s^{-1}$. For the formers, the conductivity decrease is really smooth and for $0.005\ s^{-1}$ a transition zone is observable before the conductivity decrease. For all the systems analyzed, a conductivity decrease is triggered between 0.2 and 0.5 of Hencky deformation. However, the sample extended at $0.005s^{-1}$ presents first a slight increase of the conductivity (from $4.8x10^{-3}$ S/cm to $8.2x10^{-3}$ S/cm) before the conductivity decrease starting at a higher Hencky deformation of 0.7. Moreover, its conductivity decrease is really smooth whereas at $0.1s^{-1}$, the conductivity decrease is abrupt and sudden. By dividing the extensional rate by a factor of 20, the Hencky limits ε_σ are increased by a factor greater than 2.

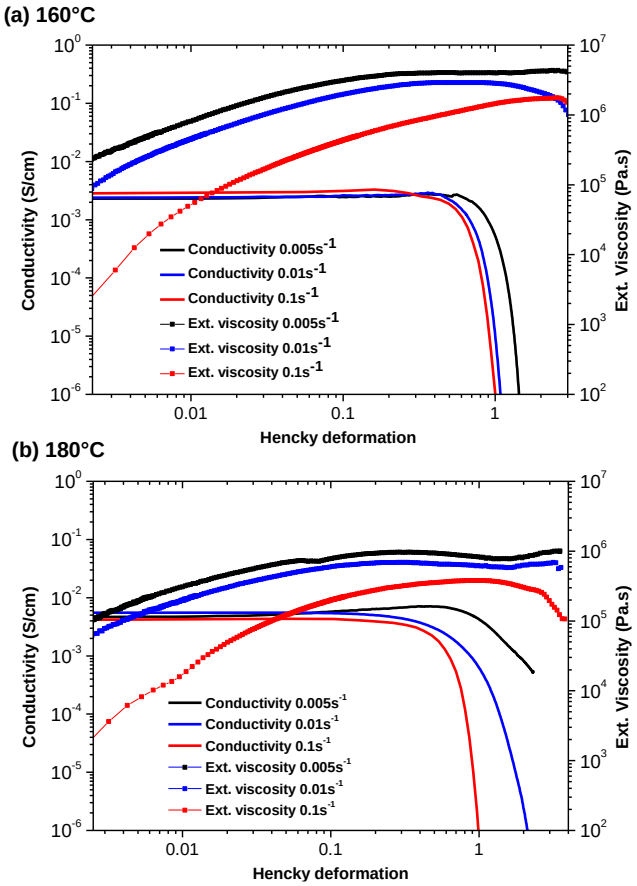

Figure 13 : Conductivity variation and extensional viscosity for 3 extensional rates (0.005 s^{-1}, 0.01 s^{-1} and 0.1 s^{-1}) at 160°C (a) and at 180°C (b) of the material PS filled with 0.79 vol% of CNT.

In Figure 14 (a), (b) and (d) are presented the structures of those three samples after a 1 Hencky deformation. The structures obtained are truly different and corroborate with the

conductivity variation. Indeed, at $0.005s^{-1}$ the structure presents no specific orientation. Conversely, the structure obtained at $0.01s^{-1}$ displays a slight orientation in the flow direction (less than the structure obtained at 160°C) and the structure obtained at $0.1s^{-1}$ is similar to the one obtained at 160°C: strong orientation within the flow direction. After a 1.7 Hencky deformation, the material deformed at an extensional rate fixed to $0.005s^{-1}$ and at 180°C (see Figure 14 (c)) presents a structure similar to those obtained after lower deformation and higher extensional rates. Those observations highlight the concomitant influences of the temperature and the extensional rate on the deformation mechanism and steer the reflection on the predominant role played by the molecular dynamics in the deformation mechanism.

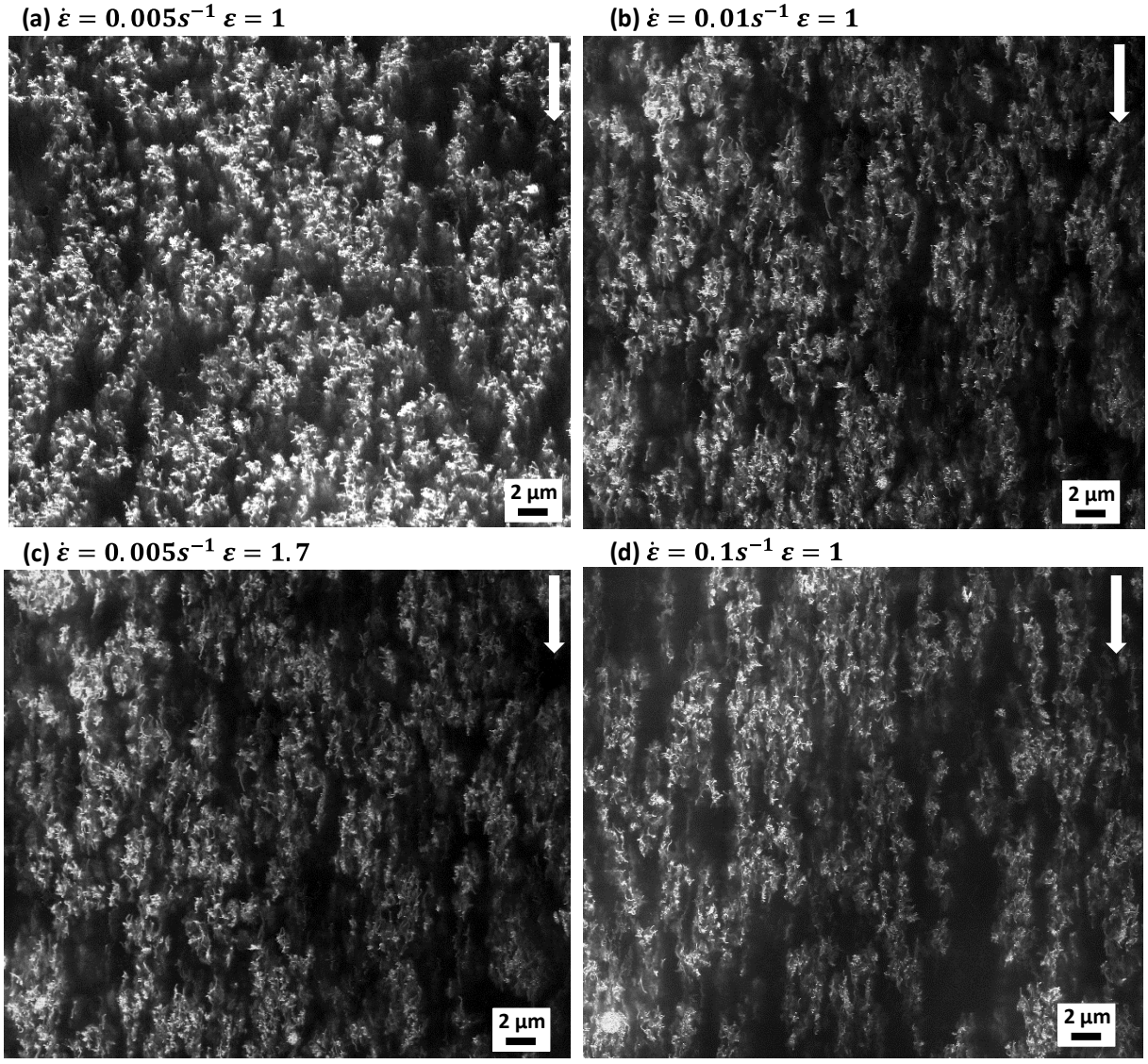

Figure 14 : SEM observation with in-Lens detector, 20 kV, WD = 5mm x2000. PS filled with 0.79vol% at 180°C extended to Hencky deformation equal to 1 at an extensional rates of $0.005s^{-1}$ (a), $0.01\ s^{-1}$ (b) and $0.1\ s^{-1}$ (d). (c) Structure obtained after 1.7 Hencky deformation at an extensional rate of $0.005s^{-1}$.

Within the flow, the polymer orientation/deformation depends on its intrinsic characteristics such as its viscosity, chains reptation, relaxation behavior etc .In extensional flow, the polymer chains are drastically oriented and/or stretched even for entangled melt. The stretching of polymer chains

competes with its relaxation. The Weissenberg number [34, 35], a dimensionless parameter defined by Equation 15 enables to quantify the main phenomenon occurring during extensional test.

$W_e = \lambda . \dot{\varepsilon}$	**Equation 15**

λ is the relaxation time and $\dot{\varepsilon}$ is the extensional rate. Commonly, the deviation from linear to non-linear behavior is ascribed to a Weissenberg number greater than 1. Here, the same convention will be taken. The different Weissenberg numbers have been determined at 160°C and 180°C for the whole range of extensional rates (Table 2) using the weight average relaxation times (see Equation 5).

Table 2 : Temperatures and extensional rates used for extensional tests and corresponding Weissenberg number W_i of the Polystyrene.

Temperature (°C)	Extensional rate (s^{-1})	Weissenberg number (W_i)
160	0.005	2.4
	0.01	4.8
	0.1	48
180	0.005	0.13
	0.01	0.26
	0.1	2.6

At 160°C all the W_i are much greater than 1. The stretch forces are predominant and the chains do not have enough time to fully relax. Moreover, the affinity between CNT and polymer chains is really strong due to strong interaction between Phenyl group and π-electron [36]. As a result, the CNT network is also oriented and stretched within the flow direction. Some experiments carried out at 140°C and not detailed in this paper also confirm the results obtained at 160°C. Contrastingly, at 180°C W_i numbers display a transition. Indeed, at $0.1s^{-1}$ W_i is greater than 1 and the CNT network is stretched and oriented within the flow. However, at $0.005s^{-1}$ and $0.01s^{-1}$ the W_i number is much lower than 1. As a result, the structure observed in SEM is significantly different (see Figure 14 (a) and (b)).

The polymer chains govern the filler network deformation. When the polymer chains can partially or fully relax, the filler network is not stretched and do not orient within the flow. The conductivity decrease is slow as the connections between aggregates are temporarily broken but conversely, the chains relaxation enables the regeneration of the inter-aggregates connections. This also explains the transition previously highlighted at extensional rate of $0.005s^{-1}$ and a temperature fixed at 180°C (see Figure 13 (b)). The slight conductivity increase observed during the extensional test can now be attributed to a more predominant connections building mechanism than connection breaking. When the deformation becomes too important the encountered stretch exceeds the entropic elasticity of the coiled chains and the connection points of the filler network begin to break slowly (see Figure 14 (c)). It can be also highlighted that some big aggregates observable in SEM are not stretched. These are generally rich in CNT so that they are very rigid. Thereupon, these CNT are not stretched.

This proposal can also explain the results obtained within rotational flow. Indeed, during steady shear experiment, Hilarius *et al*.[6] have experienced conductivity decrease until the

formation of a plateau regime and even conductivity increase. In this specific experiment, the polymer chains are stretched but significantly less than under extensional flow presented in this paper (decrease of the conductivity). The melt confinement in a constant volume and the possible chains relaxation mechanism might favor the apparition of plateau regime and instable phenomenon. In contrast, extensional deformation only drags apart the aggregates from each other.

Conclusion

This new lab scale method gives access to the monitoring of the structure variation of conductive composites under extensional deformation. With a good repeatability, this method has shown that the electrical conductor-insulator transition occurs long before the sample breaks. It also makes possible the determination of the maximal Hencky uniaxial deformation that nanocomposites can undergo before becoming electrically insulating. Moreover, it has been shown that the addition of CNT shifts the insulating transition to higher Hencky deformation. SEM characterization of the material after extensional deformation has highlighted the stretching and orientation of the CNT network.

The impact of both the temperature and the extensional rate has been investigated and has revealed the prevailing role played by the molecular dynamics in both quiescent experiment and dynamic regime. Within extensional flow, the polymer chains are stretched and oriented with the flow. Consequently, the CNT network is also stretched and oriented. In that specific case, the inter-aggregates connections are broken and the conductivity decrease is abrupt. Under appropriate conditions well described by the Weissenberg number, the polymer chains can partially or fully relax during the extensional test. This mechanism benefits to the CNT network as the aggregates are less stretched and the polymer chains relaxation triggers the inter-aggregates connection building. By consequence, the conductivity gradually decreases and the composites can undergo higher Hencky deformation before becoming electrically insulating.

Acknowledgments

This work was funded by the ANRT and Total. The authors kindly thank engineers P Alcouffe, X. Jaurand and. C Cuccuzzela for significantly help in Scanning Electronic Imaging technics and technician L. Cavetier for helping setting-up the home made EVF system.

References

1. Iijima, S., *Helical microtubules of graphitic carbon.* Nature, 1991. **354**: p. 56-58.
2. Dresselhaus M.S. , G.D., P. Avouris *Carbon Nanotubes: Synthesis, Structure, Properties and Applications.* Vol. Springer Berlin Editions. 2001.
3. Saito R. , G.D., M. S. Dresselhaus, *Physical Properties of Carbon Nanotubes*. Vol. Imperial College Press. 1998.
4. Villmow T., B.K., P.Pötschke, *Influence of screw configuration, residence time, and specific mechanical energy in twin-screw extrusion of polycaprolactone/multi-walled carbon nanotube composites.* Composites Science and Technology, 2010. **70**(14): p. 2045-2055.
5. Majid TabkhPaz, M.M., Mohammad Arjmand, *Investigation of Chaotic Mixing for MWCNT/Polymer Composites.* Marcromolecular Materials and Engineering, 2015. **300**(5): p. 482-496.

6. Hilarius K., D.L., I. Alig, T. Villmow, S. Pegel, P. Pötschke, *Influence of shear deformation on the electrical and rheological properties of combined filler networks in polymer melts: Carbon nanotubes and carbon black in polycarbonate.* Polymer, 2013. **54**(21): p. 5865-5874.
7. Cassagnau, P., *Linear viscoelasticity and dynamics of suspensions and molten polymers filled with nanoparticles of different aspect ratios.* Polymer, 2013. **54**(18): p. 4762-4775.
8. Moreira L., R.Fulchiron., G. Seytre, P. Dubois, P. Cassagnau, *Aggregation of CNT in semi dilute suspension.* Macromolecules, 2010. **43**: p. 1467-1472.
9. Tiusanen J., D.V., and J. Vuorinen, *Review on the effects of injection moulding parameters on the electrical resistivity of carbon nanotube filled polymer parts.* Composites Science and Technology, 2012. **72**(14): p. 1741-1752.
10. Alig I. P. Pötschke, D.L., T. Skipa, S. Pegel, G. R. Kasaliwal and T. Villmow, *Establishment, morphology and properties of carbon nanotube networks in polymer melts.* Polymer, 2012. **53**(1): p. 4-28.
11. Pegel S., P.P., G. Petzold, D. Lellinger, *Dispersion, agglomeration, and network formation of multiwalled carbon nanotubes in polycarbonate melts.* Polymer, 2008. **49**(4): p. 974-984.
12. Alig I., D.L., M. Engel, T. Skipa, P. Pötschke, *Destruction and formation of a conductive carbon nanotube network in polymer melts: In-line experiments.* Polymer, 2008. **49**(7): p. 1902-1909.
13. Allaoui A., S.V.H., P. Evesque, J. Baio, *Electronic transport in carbon nanotube tangles under compression: The role of contact resistance.* Scripta Materialia, 2009. **61**(6): p. 628-631.
14. Skipa T., D.L., W. Böhm, M. Saphiannikova, I. Alig, *Influence of shear deformation on carbon nanotube networks in polycarbonate melts: Interplay between build-up and destruction of agglomerates.* Polymer, 2010. **51**(1): p. 201-210.
15. Abbasi S., P.J.C., A. Derdouri, M. Moan, *Rheological properties and percolation in suspensions of multiwalled carbon nanotubes in polycarbonate.* Rheologica Acta, 2009. **48**(9): p. 943.
16. Kota, A.K., B. H. Cipriano, M. K. Duesterberg, A. L. Gershon, D. Powell, S. R. Raghavan, H. A. Bruck, *Electrical and Rheological Percolation in Polystyrene/MWCNT Nanocomposites.* Macromolecules, 2007. **40**(20): p. 7400-7406.
17. Martin C. A., J.K.W.S., M. S. P. Shaffer, M. K. Schwarz, W. Bauhofer, K. Schulte, A. H. Windle, *Formation of percolating networks in multi-wall carbon-nanotube–epoxy composites.* Composites Science and Technology, 2004. **64**(15): p. 2309-2316.
18. Marceau, S., P. Dubois, R. Fulchiron, P. Cassagnau, *Viscoelasticity of Brownian Carbon Nanotubes in PDMS Semidilute Regime.* Macromolecules, 2009. **42**(5): p. 1433-1438.
19. Abbasi S., P.J.C., A. Derdouri, *Flow induced orientation of multiwalled carbon nanotubes in polycarbonate nanocomposites: Rheology, conductivity and mechanical properties.* Polymer, 2010. **51**(4): p. 922-935.
20. Grillard F., C.J., C. Zakri, P. Miaudet, A. Derré, A. Korzhenko, P. Gaillard, P. Poulin, *Conductivity and percolation of nanotube based polymer composites in extensional deformations.* Polymer, 2012. **53**(1): p. 183-187.
21. ROUSSEAUX, D., O. Lhost, P. Lodefier, E.Scandino. *Masterbatches for preparing a composite materials with enhanced conductivity properties, process and composite materials produced*. 2015; Available from: https://www.google.com/patents/WO2015014897A1?cl=en_2.
22. Li W., S.T.B., Karl Schulte, Wolfgang Bauhofer, *The imaging mechanism, imaging depth, and parameters influencing the visibility of carbon nanotubes in a polymer matrix using an SEM.* Journal of Carbon, 2011. **49**(6).
23. Li W., W.B., *Imaging of CNTs in a polymer matrix at low accelerating voltages using a SEM.* Carbon, 2011. **49**(12): p. 3891-3898.
24. Li W., Y.Z., H.-J. Fitting, W. Bauhofer, *Imaging mechanism of carbon nanotubes on insulating and conductive substrates using a scanning electron microscope.* Journal of Materials Science, 2011(46).
25. Bird R.B., R.C.A., O. Hassager, *Dynamics of polymeric liquids. Vol. 1, 2nd Ed. : Fluid mechanics*. 1987: John Wiley and Sons Inc.,New York, NY; None. Medium: X; Size: Pages: 784.

26. Williams M. L., R.F.L., J. D. Ferry, *The Temperature Dependence of Relaxation Mechanisms in Amorphous Polymers and Other Glass-forming Liquids.* Journal of the American Chemical Society, 1955. **77**(14): p. 3701-3707.
27. Ferry, J.D., *Viscoelastic properties of polymers*. Third edition ed. 1980.
28. Cassagnau, P., J. P. Montfort, G. Marin, P. Monge, *Rheology of polydisperse polymers: relationship between intermolecular interactions and molecular weight distribution.* Rheologica Acta, 1993. **32**(2): p. 156-167.
29. Bustos F., P.C., R. Fulchiron, *Effect of molecular architecture on quiescent and shear-induced crystallization of polyethylene.* Journal of Polymer Science Part B: Polymer Physics, 2006. **44**(11): p. 1597-1607.
30. Watanabe, H., *Viscoelasticity and dynamics of entangled polymers.* Progress in Polymer Science, 1999. **24**(9): p. 1253-1403.
31. Meissner J., J.H., *A new elongational rheometer for polymer melts and other highly viscoelastic liquids.* Rheologica Acta, 1994. **33**(1): p. 1-21.
32. Zukoski IV C. F. , J.W.G., L. Marshall *Effect of electric fields on the rheology on non-aquesous concentrated suspensions* Journal of the Chemical Society, 1989. **Faraday Transaction 1**(85): p. 2785-2795.
33. Edwards S. F. , M.D., *The theory of polymer dynamics*. 1986: Oxford Press, London.
34. Somani R. H., L.Y., B. S. Hsiao, T. Sun, N. V. Pogodina, A. Lustiger, *Shear-Induced Molecular Orientation and Crystallization in Isotactic Polypropylene: Effects of the Deformation Rate and Strain.* Macromolecules, 2005. **38**(4): p. 1244-1255.
35. Elmoumni A., H.H.W., A. J. Waddon, H. Fruitwala, *Correlation of Material and Processing Time Scales with Structure Development in Isotactic Polypropylene Crystallization.* Macromolecules, 2003. **36**(17): p. 6453-6461.
36. Kin Liao, S.L., *Interfacial characteristics of CNT-PS composites system.* Applied Physical Letters, 2001. **79**.